

The Valence-Quark Distribution of the Kaon from Lattice QCD

Huey-Wen Lin,^{1,2,*} Jiunn-Wei Chen,^{3,†} Zhouyou Fan,¹ Jian-Hui Zhang,^{4,‡} and Rui Zhang^{1,2}

¹*Department of Physics and Astronomy, Michigan State University, East Lansing, MI 48824*

²*Department of Computational Mathematics, Science and Engineering,
Michigan State University, East Lansing, MI 48824*

³*Department of Physics, Center for Theoretical Physics,
and Leung Center for Cosmology and Particle Astrophysics,
National Taiwan University, Taipei, Taiwan 106*

⁴*Center of Advanced Quantum Studies, Department of Physics,
Beijing Normal University, Beijing 100875, China*

We present the first lattice-QCD calculation of the kaon valence-quark distribution functions using the large-momentum effective theory (LaMET) approach, a method that has been applied to a wide variety of isovector nucleon distributions and valence pion distributions. This is the first such lattice calculation with multiple pion masses with the lightest one around 220 MeV, 2 lattice spacings $a = 0.06$ and 0.12 fm, $(M_\pi)_{\min}L \approx 5.5$, and high statistics ranging from 11,600 to 61,312 measurements. We also find the valence-quark distribution of pion to be consistent with the FNAL E615 experimental results. Our ratio of the u quark PDF in the kaon to that in the pion agrees with the CERN NA3 experiment. We make predictions of the strange quark distribution of the kaon.

PACS numbers: 12.38.-t, 11.15.Ha, 12.38.Gc

I. INTRODUCTION

Light pseudoscalar mesons play a fundamental role in QCD since they are the Nambu-Goldstone bosons associated with dynamical chiral symmetry breaking (DCSB), and thereby provide a useful testing ground for our understanding of nonperturbative QCD. While studies of pion and kaon structures both reveal physics of DCSB, a comparison between them helps to reveal the relative impact of DCSB versus the explicit breaking of chiral symmetry by the quark masses.

The parton distribution functions (PDFs) are important quantities characterizing the structure of the pion and kaon. They can be measured by scattering a secondary pion (π) or kaon (K) beam over target nuclei (A), inducing the Drell-Yan process, $\pi(K)A \rightarrow X\mu^+\mu^-$, where the muon (μ) pair is detected but not the rest of the final state (X) [1–5]. With a combined analysis of π^+A and π^-A Drell-Yan on the same nuclear target, the valence and sea distributions can be separated [1], provided the nuclear PDF is known. Currently, the nuclear PDFs are approximated by a combination of proton and neutron PDFs; the remaining nuclear modifications must then be quantified by combined efforts from theory and experiment. The valence-quark PDF of the pion for momentum fraction $x \gtrsim 0.2$ has been determined reasonably well [1, 2, 5–7], subject to the systematic uncertainty in the PDF parametrization.

Combining K^-A and π^-A Drell-Yan data, the kaon valence PDF can be measured through the ratio [8]

$\bar{u}_v^{K^-}(x)/[\bar{u}_v^{\pi^-}(x)C(x)]$ where $\bar{u}_v^{K^-}(\pi^-)$ denotes the valence anti-up distribution in the K^- (π^-). The function $C(x)$ encodes the corrections needed due to the nuclear modification of the target PDFs, the omission of meson sea-quark distributions and the ignorance of the ratio $s_v^{K^-}(x)/\bar{u}_v^{K^-}(x)$. In principle, the first two can be addressed by new experiments. For example, the valence and sea PDFs for the pion and kaon at $x > 0.2$ can be separated in the π^\pm and K^\pm Drell-Yan experiments proposed by the COMPASS++/AMBER collaboration using the CERN M2 beamline [9]. Numerically, the biggest uncertainty in $C(x)$ is due to ignorance of the $s_v^{K^-}(x)/\bar{u}_v^{K^-}(x)$ ratio, and a reliable theoretical determination of this ratio, e.g. by lattice QCD, would greatly reduce the uncertainty in $\bar{u}_v^{K^-}(x)/\bar{u}_v^{\pi^-}(x)$.

To understand the importance of $C(x)$, consider, for example, the PDFs at $x = 0.9$; if one uses a conservative estimation $1 < s_v^{K^-}(x)/\bar{u}_v^{K^-}(x) < 10$ then $1 > C(x) > 0.85$, although $C(x)$ is very close to unity at $x = 0.2$ [8]. With this estimation of $C(x)$, $\bar{u}_v^{K^-}(x) < \bar{u}_v^{\pi^-}(x)$ is observed for $x > 0.7$. The smallness of \bar{u} in K^- relative to π^- at large x can be understood in the limit where the strange-quark mass is very heavy ($m_s \rightarrow \infty$). In this heavy-quark limit, no strange sea quarks are produced, and all the momentum of K^- must be carried by the valence strange quark, so \bar{u} is highly skewed towards small x . At physical m_s , the effects of the strange sea quarks are not negligible. Although one can still think about a dressed quark as an effective valence quark, it is not clear whether this notion of effective valence quark is a good approximation to the valence quark in full QCD. Therefore, whether $\bar{u}_v^{K^-}(x) < \bar{u}_v^{\pi^-}(x)$ at large x for physical quark masses is an interesting and nontrivial theoretical problem that we would like to address using lattice QCD.

Another experiment that could measure the pion and

*Electronic address: hwlin@pa.msu.edu

†Electronic address: jwc@phys.ntu.edu.tw

‡Electronic address: zhangjianhui@bnu.edu.cn

kaon PDFs is tagged deep inelastic scattering (TDIS), such as $ep \rightarrow e'(n \text{ or } Y)X$. By tagging a neutron (n) or hyperon (Y) with specific kinematics in the final state of an electron (e) scattering on a proton (p), one can select events of the Sullivan process [10], where an electron scatters off an intermediate t -channel pion or kaon. Unlike the Drell-Yan experiment, whose theoretical error can be systematically studied by QCD factorization, the Sullivan-process approach relies on the validity of the meson-cloud model [11–13]. It is unclear how to quantify the theoretical uncertainty systematically in this approach. Although the meson-cloud model was made systematic using chiral perturbation theory for inclusive processes such as DIS [14–17], it is not clear whether it can be applied to TDIS processes as well. Experimentally, the tagged-neutron DIS experiment was pioneered by HERA, covering $x < 0.01$ [18]. Approved experiments at JLab aim to determine $\bar{u}_v^{\pi^-}$ for $x > 0.45$ with better than 1.1% statistical and 6.5% systematic uncertainty [19] and to determine $\bar{u}_v^{K^-}$ in the same range with 3% statistical and 6.5% systematic uncertainty [20]. The combined result will determine the ratio with 3% statistical and 5% systematic uncertainty [20]. At future Electron-Ion Collider (EIC), TDIS experiments can cover the from $x = 10^{-3}$ with $Q^2 = 1 \text{ GeV}^2$ to $x = 1$ with $Q^2 = 1000 \text{ GeV}^2$. The statistical uncertainty of the ratio $\bar{u}_v^{K^-}(x)/\bar{u}_v^{\pi^-}(x)$ can be reached to 1–3% level for $x \in [0.2, 0.9]$ with about 5% statistical uncertainty [21].

Since there is a great experimental interest and effort to probe the pion and kaon PDFs, it is timely that these quantities have recently become calculable in lattice QCD, thanks to the development of large-momentum effective theory (LaMET) [22, 23]. This theory provides a general framework to extract lightcone correlations, such as the PDFs of hadrons, from equal-time Euclidean correlations calculable on the lattice. The latter can be computed at a moderately large hadron momentum, and then converted to the former through factorization formulas accurate up to power corrections that are suppressed by the hadron momentum.

Since its proposal, LaMET has been applied to compute various nucleon PDFs [24–33], the pion PDF and GPDs [34, 35], as well as the meson distribution amplitudes [36, 37], yielding encouraging results. In particular, the state-of-the-art calculation of the unpolarized and polarized isovector quark PDF of the nucleon [32, 38] agrees with the global PDF fits [39–43] within errors. There have also been ongoing efforts to achieve full control of lattice systematics, including an analysis of finite-volume systematics [33] and exploration of machine-learning application [44] that have been carried out recently. In parallel with the progress using LaMET, other proposals to calculate the PDFs in lattice QCD have also been formulated and applied to various parton quantities [45–53]. Of course, each of them is subject to its own systematics.

In this paper, we carry out the first lattice-QCD calculation of the valence-quark distribution of the kaon using LaMET. Our calculation is done using clover valence

fermions on an ensemble of gauge configurations with $N_f = 2 + 1 + 1$ (degenerate up/down, strange and charm) flavors of highly improved staggered quarks (HISQ) [54], generated by the MILC Collaboration [55] with two lattice spacings $a = 0.06$ and 0.12 fm and three pion masses, approximately 690, 310 and 220 MeV.

II. KAON PDF FROM LAMET LATTICE CALCULATION

To see how the quark PDF in the kaon can be obtained within LaMET, we begin with the following operator definition

$$q^K(x) = \int \frac{d\lambda}{4\pi} e^{-ix\lambda n \cdot P} h_{\not{n}}(\lambda n) \\ = \int \frac{d\lambda}{4\pi} e^{-ix\lambda n \cdot P} \langle K(P) | \bar{\psi}_q(\lambda n) \not{n} W(\lambda n, 0) \psi_q(0) | K(P) \rangle, \quad (1)$$

where $|K(P)\rangle$ denotes a kaon state with momentum $P^\mu = (P_0, 0, 0, P_z)$, $\psi_q, \bar{\psi}_q$ are the quark fields of flavor q , n^μ is a unit direction vector and

$$W(\zeta n, \eta n) \equiv \exp\left(ig \int_\eta^\zeta d\rho n \cdot A(\rho n)\right) \quad (2)$$

is the gauge link inserted to ensure gauge invariance. For later convenience, we have used a subscript \not{n} on h to denote the Dirac structure sandwiched between the quark fields. If we choose lightlike $n = n_+ = (1, 0, 0, -1)/\sqrt{2}$, then Eq. 1 defines the usual quark PDF with x denoting the fraction of kaon momentum carried by the quark. The support of x is $[-1, 1]$ with the negative x part corresponding to the antiquark distribution: $\bar{q}^K(x) = -q^K(-x)$ for $x > 0$. One can define the valence-quark distribution for the positive range as $q_v^K(x) = q^K(x) - \bar{q}^K(x)$, which satisfies $\int_0^1 dx q_v^K(x) = 1$ for a quark of the appropriate flavor.

On the other hand, if we choose spacelike $n = \tilde{n} = (0, 0, 0, -1)$, then Eq. 1 becomes a Euclidean correlator known as quasi-PDF, which can be calculated in lattice QCD. The idea behind LaMET is that for a given momentum $P_z \gg \Lambda_{\text{QCD}}$, the quasi-PDF has the same infrared physics as the PDF, so the two quantities can be connected via a factorization formula. Such a factorization can be done with either bare or renormalized correlators. We will follow the latter, since it facilitates the conversion from lattice results to results in the continuum.

On the lattice, we first calculate the quasi-PDF matrix element in coordinate space, and then renormalize it nonperturbatively in a conventional scheme such as the regularization-independent momentum-subtraction (RI/MOM) scheme. To avoid potential mixing with scalar operators, we replace the Dirac structure \not{n} with $\tilde{\not{n}}_t$, where $\tilde{n}_t = (1, 0, 0, 0)$. The RI/MOM renormalization

factors Z can then be determined by demanding that it cancels all the loop contributions for the matrix element in an off-shell external quark state at a specific momentum [30, 56]:

$$h_{\tilde{n}_t, R}(\lambda\tilde{n}) = Z^{-1}(p_z^R, 1/a, \mu_R) h_{\tilde{n}_t}(\lambda\tilde{n}), \quad (3)$$

with

$$Z(p_z^R, 1/a, \mu_R) = \frac{\text{Tr}[\not{p} \sum_s \langle p, s | \bar{\psi}_f(\lambda\tilde{n}) \not{\gamma}_t W(\lambda\tilde{n}, 0) \psi_f(0) | p, s \rangle]}{\text{Tr}[\not{p} \sum_s \langle p, s | \psi_f(\lambda\tilde{n}) \not{\gamma}_t W(\lambda\tilde{n}, 0) \psi_f(0) | p, s \rangle_{\text{tree}}]} \Big|_{\substack{p^2 = -\mu_z^2 \\ p_z = p_z^R}}. \quad (4)$$

After renormalization and taking the continuum limit, $h_{\tilde{n}_t, R}(\lambda\tilde{n})$ can be converted to the lightcone PDFs via the factorization

$$q^K(x, \tilde{n}, \tilde{\mu}) = \int \frac{dy}{|y|} C\left(\frac{x}{y}, \frac{\tilde{\mu}}{\mu}, \frac{\mu}{yP_z}\right) \tilde{q}^K(y, n_+, \mu) + \mathcal{O}\left(\frac{m_K^2}{P_z^2}, \frac{\Lambda_{\text{QCD}}^2}{x^2 P_z^2}\right), \quad (5)$$

where C is a perturbative matching kernel converting the RI-MOM renormalized quasi-distribution to the one in $\overline{\text{MS}}$ scheme used in our previous works [32, 34, 35, 38].

In this work we use clover valence fermions with $N_f = 2 + 1 + 1$ (degenerate up/down, strange and charm) flavors of highly improved staggered dynamical quarks (HISQ) [54] in the sea, on ensembles generated by MILC Collaboration [55]. We use one step of hypercubic (HYP) smearing on the gauge links [57] to suppress discretization effects, and the fermion-action parameters are tuned to recover the lowest pion mass of the staggered quarks in the sea. Details can be found in Refs. [58–61]. We note that no exceptional configurations have been found among all the ensembles we use in this work [58–61]. The multigrid algorithm [62, 63] in the Chroma software package [64] is used to speed up the clover fermion inversion of the quark propagators. We use Gaussian momentum smearing [65] for both the light- and strange-quark fields $\psi(x) + \alpha \sum_j U_j(x) e^{ik\hat{e}_j} \psi(x + \hat{e}_j)$, where k is the input momentum-smearing parameter, $U_j(x)$ are the gauge links in the j direction, and α is a tunable parameter as in traditional Gaussian smearing. Table I summarizes the momenta, source-sink separations, and statistics used in this work.

On the lattice, we calculate both two-point and three-point correlators. We test on the meson unpolarized quasi-PDF measurements on the lattice:

$$C_{2\text{pt}}(t_{\text{sep}}, \vec{P}) = \langle 0 | \int d^3\vec{y} e^{i\vec{y}\cdot\vec{P}} \overline{M}_{\text{ps}}(\vec{y}, t_{\text{sep}}) M_{\text{ps}}(\vec{0}, 0) | 0 \rangle, \quad (6)$$

$$C_{3\text{pt}}(z, t, t_{\text{sep}}, \vec{P}) = \langle 0 | \int d^3y e^{i\vec{y}\cdot\vec{P}} \overline{M}_{\text{ps}}(\vec{y}, t_{\text{sep}}) \times \bar{q}(z\hat{z}, t) \Gamma \prod_{x=0}^{z-1} U_z(x\hat{z}, t) q(\vec{0}, t) M_{\text{ps}}(\vec{0}, 0) | 0 \rangle, \quad (7)$$

where $C_{3\text{pt}}$ is the three-point correlator with $q = \{l, s\}$ quarks, $C_{2\text{pt}}$ is the two-point correlator, $M_{\text{ps}} = \bar{q}_1 \gamma_5 q_2$ is the pseudoscalar meson operator with $q_{1,2}$ being either the light- or strange-quark operator, z is the length of the Wilson line, $U_\mu(\vec{x}, t)$ is a lattice gauge link. For the unpolarized meson PDFs, we choose Dirac spinor matrices $\Gamma = \gamma_t$ here as suggested in Refs. [66, 67] to avoid mixing with the scalar matrix element. t and t_{sep} are the operator-insertion time and source-sink separation. We choose the meson boost momentum \vec{P} to lie along the z direction and denote its magnitude P_z . All the source locations are randomly selected for each configuration; we shift to $t = 0$ for convenience before the measurements are averaged.

The matrix elements for the meson PDF are then extracted using multiple source-sink separations t_{sep} , removing excited-state contamination by performing “two-simRR” fits [61]:

$$C_\Gamma^{3\text{pt}}(P_z, t, t_{\text{sep}}) = |\mathcal{A}_0|^2 \langle 0 | \mathcal{O}_\Gamma | 0 \rangle e^{-E_0 t_{\text{sep}}} + \mathcal{A}_1 \mathcal{A}_0^* \langle 1 | \mathcal{O}_\Gamma | 0 \rangle e^{-E_1(t_{\text{sep}}-t)} e^{-E_0 t} + \mathcal{A}_0 \mathcal{A}_1^* \langle 0 | \mathcal{O}_\Gamma | 1 \rangle e^{-E_0(t_{\text{sep}}-t)} e^{-E_1 t} + |\mathcal{A}_1|^2 \langle 1 | \mathcal{O}_\Gamma | 1 \rangle e^{-E_1 t_{\text{sep}}} + \dots \quad (8)$$

at each meson boost momentum. The E_0 (E_1) and \mathcal{A}_0 (\mathcal{A}_1) are the ground- (excited-) state nucleon energy and overlap factors, extracted from the two-point correlators by fitting them to the form

$$C^{2\text{pt}}(P_z, t_{\text{sep}}) = |\mathcal{A}_0|^2 e^{-E_0 t_{\text{sep}}} + |\mathcal{A}_1|^2 e^{-E_1 t_{\text{sep}}} + \dots \quad (9)$$

A few selected fits to the three-point ratio

$$R_V(t_{\text{sep}}, t) = \frac{C_{3\text{pt}}(t_{\text{sep}}, t)}{C_{2\text{pt}}(t_{\text{sep}})} \quad (10)$$

are plotted from a subset of data on all three ensembles with $P_z = 5 \times 2\pi/L$ from the a12m220L ensemble in Fig. 1; these use different t_{sep} , with source-sink separations from 0.72 fm to 1.08 fm. The upper-left plot shows “two-simRR” fits, where all t_{sep} are fit simultaneously to all terms listed in Eq. 8, while the rest of the plots show fits without the $\langle 1 | \mathcal{O}_\Gamma | 1 \rangle$ term; the extracted ground-state matrix elements are consistent between these two analysis methods. We also examine the fitted ground-state matrix elements from a two-state fit to each t_{sep} in the upper-right and bottom plots. The extracted ground-state matrix elements are also consistent among different t_{sep} , and agree with the simultaneous fits using all t_{sep} . The signal-to-noise ratio deteriorates significantly as t_{sep} is increased, even though we have increased the number of measurements at larger

Ensemble ID	a (fm)	$N_s^3 \times N_t$	M_π^{val} (MeV)	$M_{\eta_s}^{\text{val}}$ (MeV)	$M_\pi^{\text{val}} L$	t_{sep}/a	P_z	N_{cfg}	N_{meas}
a12m310	0.12	$24^3 \times 64$	310	683	4.55	{6, 7, 8, 9}	$\{3\} \frac{2\pi}{L}$	958	{22922, 45984, 45984, 61312}
a12m220L	0.12	$40^3 \times 64$	217	687	5.5	{6, 7, 8, 9}	$\{4, 5\} \frac{2\pi}{L}$	840	{13440, 26800, 26800, 53760}
a06m310	0.06	$48^3 \times 96$	319	690	4.52	{12, 14, 16, 18}	$\{3\} \frac{2\pi}{L}$	725	{11600, 23200, 23200, 46400}

TABLE I: Ensemble information and parameters used in this calculation. N_{meas} corresponds to the total number of measurements of the three-point correlators for $t_{\text{sep}} = \{0.72, 0.84, 0.96, 1.08\}$ fm, respectively.

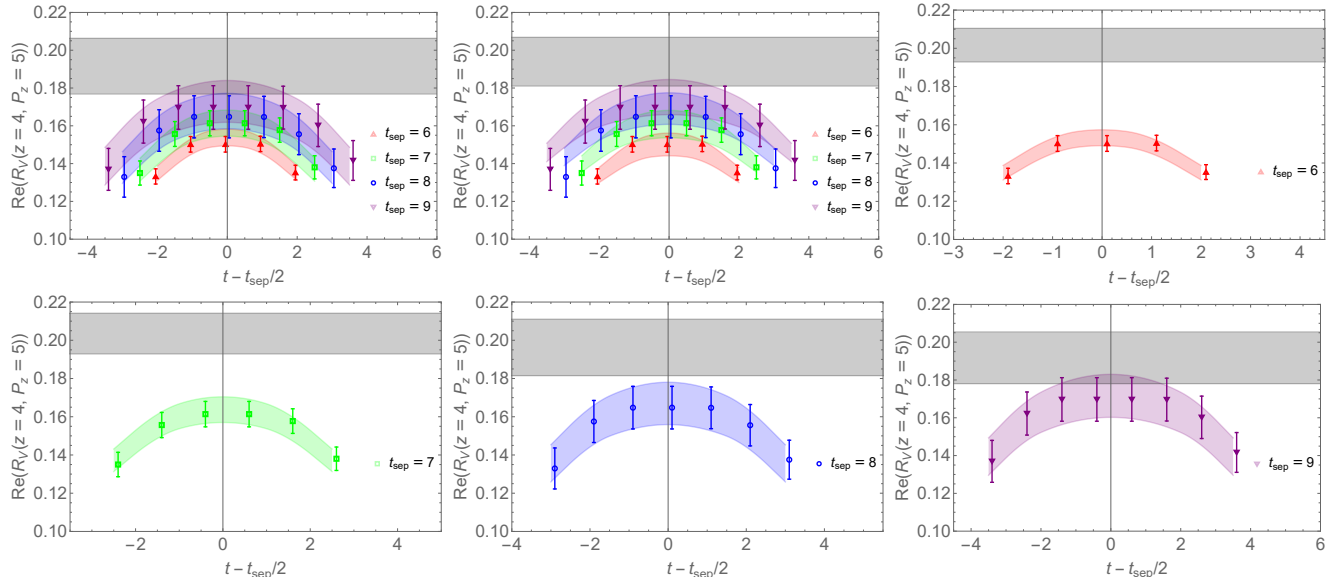


FIG. 1: Example plots of the ratio of three- to two-point correlators as functions of the insertion time t from the a12m220L ensemble. The real parts of the matrix elements are shown for kaon momentum $P_z \approx 1.7$ GeV and length of the Wilson line $z/a = 4$, with curved bands showing fits using different source-sink separations $t_{\text{sep}}/a \in \{6, 7, 8, 9\}$. The gray bands indicate the final extracted ground-state matrix elements. The upper-left two plots show the fitted ratios R and their corresponding ground-state matrix elements obtained via the “two-simRR” (“two-sim”) method, while the rest of the plots are “two-state” fits using only one t_{sep} . The ground-state extractions are consistent across different choices of source-sink three-point inputs, as well as across different choices of analysis method.

source-sink separations. One can clearly see that the simultaneous fits well describe data from all t_{sep} , and the errors in the final extracted ground-state matrix-element extraction are not over-constrained by the smallest t_{sep} data. For the remainder of the paper, we only use the “two-sim” fits to obtain ground-state matrix elements for further processing. An example result from one of the ensembles is shown in Fig. 2. We find that the extractions of the ground-state matrix elements are stable across different fit-range choices among two-point and three-point correlators.

III. RESULTS AND DISCUSSION

In this work, we choose $\mu^R = 2.4$ GeV and $p_z^R = 0$ to compute the RI/MOM renormalization factors defined in Eq. 4. With $p_z^R = 0$, the renormalization factors are real. They are calculated from all three ensembles and are shown in Fig. 3. The renormalization factors are

counterterms to cancel the UV divergence of the bare matrix elements; hence, they are sensitive to the UV cutoff or lattice spacing but not sensitive to the pion mass.

We summarize the renormalized kaon valence-quark matrix elements in Fig. 4. Only the real parts of the matrix elements are shown, because $q_v^K(|x|) = q^K(|x|) - \bar{q}^K(|x|) = q^K(|x|) + q^K(-|x|)$, and by Eq. 1 only the real parts of the matrix elements contribute to the valence distribution. The matrix elements shown here are normalized by the corresponding mean value of the calculated vector charge so that one can easily compare the zP_z dependence. The pion-mass dependence of the matrix elements is small for the two $a \approx 0.12$ fm ensembles with 220 and 310 MeV pion mass points. The lattice-spacing dependence between $a \approx 0.06$ and 0.12 fm is benign in most regions of zP_z , but the trend starts to diverge between these two lattice spacing results for $zP_z > 5$. They remain within two standard deviations. For the rest of this work, we will neglect the lattice-spacing dependence.

Next, we perform a chiral extrapolation to obtain the

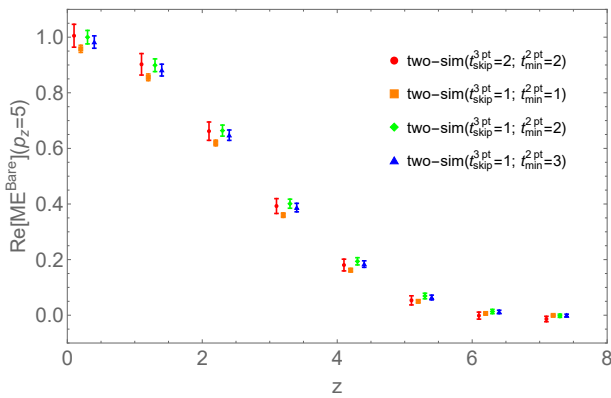


FIG. 2: Comparison of the fitted kaon ground-state matrix elements as functions of Wilson-line length z (in lattice units) from the a12m220L ensemble with $P_z \approx 5 \times \frac{2\pi}{L}$ and pion mass of 220 MeV using “two-sim” fits and varying the fit range of the two-point (t_{\min}^{2pt} corresponding to fit range of $[t_{\min}^{2pt}, N_t/4]$) and three-point correlators (t_{\min}^{3pt} corresponding to fit range of $[t_{\min}^{3pt}, t_{\text{sep}} - t_{\text{skip}}^{3pt}]$).

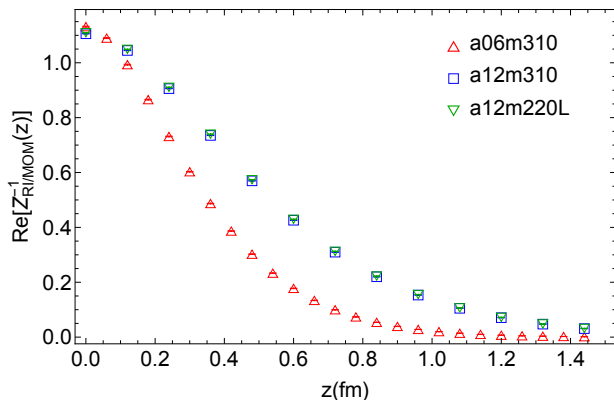


FIG. 3: The inverse renormalization constant from all three ensembles as functions of Wilson-line displacement z with RI/MOM renormalization scales $\mu_R = 2.4$ GeV and $p_z^R = 0$. The dependence of the renormalization constants on pion mass is negligible, but the dependence on lattice spacing is significant.

renormalized matrix elements at physical pion mass. We use a simple ansatz to combine our data from 220, 310 and 690 MeV: $h_i^R(P_z, z, M_\pi) = c_{0,i} + c_{1,i}M_\pi^2$ with $i = K, \pi$. The extrapolation plots can be found in Fig. 5, where the results from individual pion masses are shown as lines, while the extrapolated results at physical pion mass are shown as pink bands. Overall, the extrapolated matrix elements are consistent with the 310- and 220-MeV results, but can be significantly different from the 690-MeV ones.

With the matrix elements at physical pion-mass, we obtain the pion and kaon PDFs through Eq. 5, as proposed for the pion valence PDF in Ref. [68]. We take the

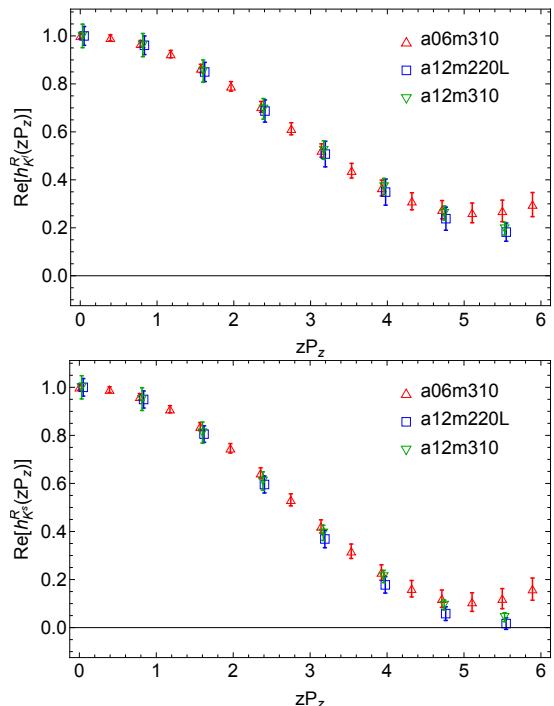


FIG. 4: The renormalized matrix elements of the light (top) and strange (bottom) valence-quark contributions to the kaon PDFs as functions of dimensionless zP_z . The renormalization scales are fixed at $\mu_R = 2.4$ GeV and $p_z^R = 0$. We observe no significant pion-mass nor lattice-spacing dependence in most regions of the calculated zP_z .

commonly used analytical form

$$f_{m,n}(x) = \frac{x^m(1-x)^n}{B(m+1, n+1)}, \quad (11)$$

where $B(m+1, n+1) = \int_0^1 dx x^m(1-x)^n$ is the beta function, which normalizes the distribution such that the area under the curve is unity. The RI/MOM renormalized quasi-PDF can be matched to the $\overline{\text{MS}}$ renormalized PDF using the matching kernel defined in Ref. [38] with the meson-mass correction from Ref. [25].

Our fit using Eq. 11 and Eq. 5 is good with $\chi^2/\text{dof} = 0.27$. The leading moments from the pion distribution are $\langle x \rangle_v = 0.289(23)$, $\langle x^2 \rangle_v = 0.144(18)$, $\langle x^3 \rangle_v = 0.088(15)$, which are consistent with the traditional moment approach done by ETMC using $N_f = 2 + 1 + 1$ twisted-mass fermions with pion masses in the range of 230 to 500 MeV, renormalized at 2 GeV; see Table V in Ref. [69] with $\langle x \rangle$ ranging 0.23–0.29 and $\langle x^2 \rangle$ ranging 0.11–0.18. Figure 6 shows our final results for the pion valence distribution at physical pion mass (u_v^+) multiplied by Bjorken- x as a function of x . We evolve our results to a scale of 27 GeV² using the NNLO DGLAP equations from the Higher-Order Perturbative Parton Evolution Toolkit (HOPPET) [70] to compare with other results. When comparing with the results from experimental data, our result is consistent with the original

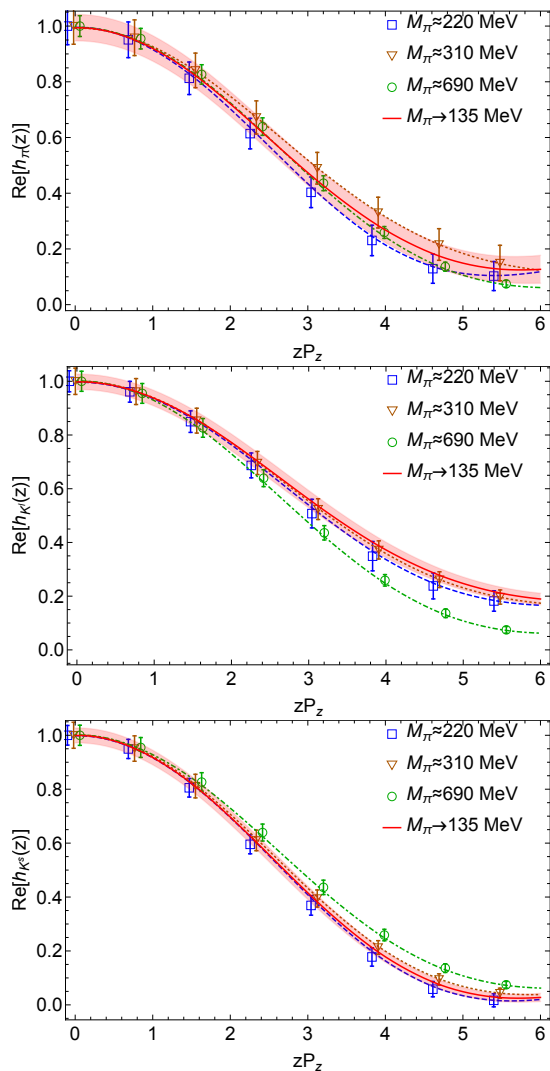


FIG. 5: The extrapolation in pion mass of the renormalized matrix elements of the pion (top), and light (middle) and strange (bottom) valence-quark contributions to the kaon PDFs as functions of dimensionless zP_z . The lines indicate the central values of the fits to the matrix elements at individual pion masses. The pink bands show the uncertainties of the results after extrapolation to the physical pion mass.

analysis of the FNAL-E615 experiment data [5] with our result approaching large- x with $\sim (1-x)^{1.01}$, whereas there is tension with the $x > 0.6$ distribution from the reanalysis of the FNAL-E615 experiment data using next-to-leading-logarithmic threshold resummation effects in the calculation of the Drell-Yan cross section [7] (labeled as “ASV’10”), which agree better with the distribution from Dyson-Schwinger equations [71]; both prefer $\sim (1-x)^2$ as $x \rightarrow 1$. An independent lattice study of the pion valence-quark distribution [72], also extrapolated to physical pion mass, using the “lattice cross sections” (LCSs) [45], reported similar results to ours. Our lowest 3 moments at the scale of 27 GeV^2 are 0.230(18), 0.102(13), 0.057(10), which are consistent with the mo-

ments (0.23, 0.094, 0.048) from chiral constituent quark model [73].

Figure 7 shows the ratios of the light-quark distribution in the kaon to the one in the pion ($u_v^{K^+}/u_v^{\pi^+}$). When comparing our result with the original experimental determination of the valence quark distribution via the Drell-Yan process by NA3 Collaboration [1] in 1982, we found good agreement between our results and the data. Our result approaches 0.4 as $x \rightarrow 1$ and agrees nicely with other analyses, such as constituent quark model [74], the Dyson-Schwinger equations (DSE) approach (“DSE’11”) [75], and basis light-front quantization with color-singlet Nambu–Jona-Lasinio interactions (“BLFQ-NJL’19”) [76]. Our lowest 3 moments for $u_v^{K^+}$ are 0.193(8), 0.080(7), 0.042(6), respectively, which are close to the QCD model estimates of 0.23, 0.091, 0.045 from chiral constituent quark model [73] and 0.28, 0.11, 0.048 from Dyson-Schwinger equations [71]. Our prediction for xs_v^K is also shown in Fig. 7 with the lowest 3 moments of s_v^K being 0.267(8), 0.123(7), 0.070(6), respectively; the moment results are within the ranges of the QCD model estimates from chiral constituent quark model [73] (0.24, 0.096, 0.049) and Dyson-Schwinger equations [71] (0.36, 0.17, 0.092).

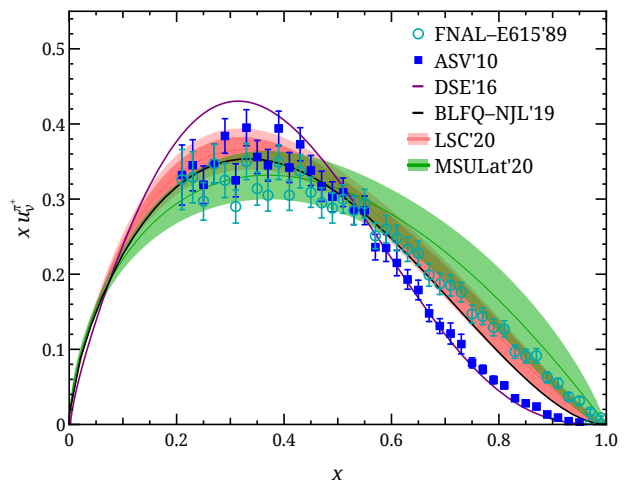


FIG. 6: Summary comparison of xu_v^π as a function of x at scale of 27 GeV^2 : our result at physical pion mass (labeled “MSULat’20”, shown as a green band), another lattice work using lattice good cross-section method (“LSC’20”, shown as a red band) [72] at physical pion mass, along with the original analysis of the FNAL-E615 experiment data [5] (“FNAL-E615’89”, cyan circles) and the reanalysis (“ASV’10”, blue squares) [7] which agree perfectly with the distribution obtained from Dyson-Schwinger equations (“DSE’16”) [71], the obtained from basis light-front quantization with NJL interactions (“BLFQ-NJL’19”).

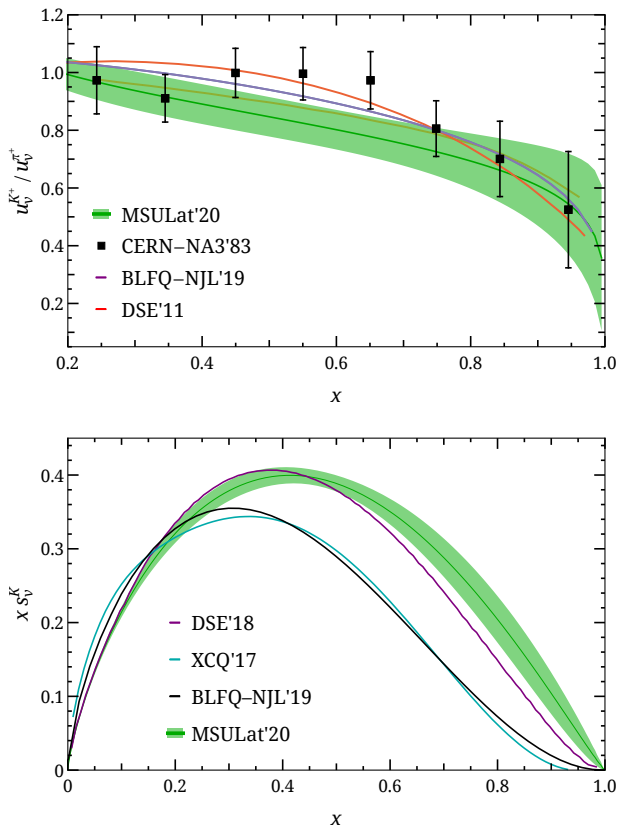


FIG. 7: (Top) The ratio of the light-quark valence distribution of kaon to that of pion from this work (labeled “MSULat’20”), along with the results of the CERN NA3 experiment [1], the next-leading-order of Gluck-Reya-Stratmann model [74] (“GRS’97”), the DSE approach (“DSE’11”) [75], and one obtained from basis light-front quantization with NJL interactions (“BLFQ-NJL’19”) [76]. (Bottom) Our result for $x s_v^K(x)$ (labeled “MSULat’20”) as function of x , along with that from chiral constituent quark model [73] (“XCQ’17”), the one obtained from basis light-front quantization with NJL interactions [77] (“BLFQ-NJL’19”), and one obtained from using rainbow-ladder truncation of QCD Dyson-Schwinger equations [78] (“DSE’18”)

IV. CONCLUSION

In this work, we presented the first direct lattice-QCD calculation of the x dependence of the kaon parton dis-

tribution functions using two lattice spacings, multiple pion masses ($M_{\pi, \min} = 217$ MeV) and $M_{\pi}L \in \{4.5, 5.5\}$ with high statistics, $N_{\text{meas}} \in \{11, 61\}$ thousands and $N_{\text{cfg}} \in \{725, 958\}$. Our valence-quark pion distribution is in good agreement with the one obtained by JLab/W&M group using LSC methods and extrapolated to the physical pion mass. The ratios of the light-quark valence distribution in the kaon to the one in pion, u_v^K / u_v^{π} , were found to be consistent with the original CERN NA3 experiments. We made predictions for the strange-quark valence distribution of the kaon, $s_v^K(x)$, determining that it is close to the DSE result [78].

Acknowledgments

We thank the MILC Collaboration and RBC Collaboration for sharing the lattices used to perform this study. The LQCD calculations were performed using the Chroma software suite [64]. This research used resources of the National Energy Research Scientific Computing Center, a DOE Office of Science User Facility supported by the Office of Science of the U.S. Department of Energy under Contract No. DE-AC02-05CH11231 through ERCAP; facilities of the USQCD Collaboration, which are funded by the Office of Science of the U.S. Department of Energy, and supported in part by Michigan State University through computational resources provided by the Institute for Cyber-Enabled Research (iCER). ZF, HL and RZ are supported by the US National Science Foundation under grant PHY 1653405 “CAREER: Constraining Parton Distribution Functions for New-Physics Searches”. JWC is partly supported by the Ministry of Science and Technology, Taiwan, under Grant No. 108-2112-M-002-003-MY3 and the Kenda Foundation. JHZ is supported in part by National Natural Science Foundation of China under Grant No. 11975051, and by the Fundamental Research Funds for the Central Universities.

[1] J. Badier et al. (NA3), *Z. Phys.* **C18**, 281 (1983).
 [2] B. Betev et al. (NA10), *Z. Phys.* **C28**, 9 (1985).
 [3] S. Falciano et al. (NA10), *Z. Phys.* **C31**, 513 (1986).
 [4] M. Guanziroli et al. (NA10), *Z. Phys.* **C37**, 545 (1988).
 [5] J. S. Conway et al., *Phys. Rev.* **D39**, 92 (1989).
 [6] K. Wijesooriya, P. E. Reimer, and R. J. Holt, *Phys. Rev.* **C72**, 065203 (2005), nucl-ex/0509012.
 [7] M. Aicher, A. Schafer, and W. Vogelsang, *Phys. Rev.*

Lett. **105**, 252003 (2010), 1009.2481.
 [8] J. Badier et al. (Saclay-CERN-College de France-Ecole Poly-Orsay), *Phys. Lett.* **93B**, 354 (1980).
 [9] B. Adams et al. (2018), 1808.00848.
 [10] J. D. Sullivan, *Phys. Rev.* **D5**, 1732 (1972).
 [11] J. Speth and A. W. Thomas, *Adv. Nucl. Phys.* **24**, 83 (1997), [83(1996)].
 [12] P. L. McGaughey, J. M. Moss, and J. C. Peng, *Ann. Rev.*

- Nucl. Part. Sci. **49**, 217 (1999), hep-ph/9905409.
- [13] S. Kumano, Phys. Rept. **303**, 183 (1998), hep-ph/9702367.
- [14] D. Arndt and M. J. Savage, Nucl. Phys. **A697**, 429 (2002), nucl-th/0105045.
- [15] J.-W. Chen and X.-d. Ji, Phys. Lett. **B523**, 107 (2001), hep-ph/0105197.
- [16] J.-W. Chen and X.-d. Ji, Phys. Rev. Lett. **87**, 152002 (2001), [Erratum: Phys. Rev. Lett.88,249901(2002)], hep-ph/0107158.
- [17] J.-W. Chen and X.-d. Ji, Phys. Rev. Lett. **88**, 052003 (2002), hep-ph/0111048.
- [18] F. D. Aaron et al. (H1), Eur. Phys. J. **C68**, 381 (2010), 1001.0532.
- [19] D. Adikaram et al., Measurement of Tagged Deep Inelastic Scattering (TDIS), approved Jefferson Lab experiment E12-15-006 (2015).
- [20] D. Adikaram et al., Measurement of Kaon Structure Function through Tagged Deep Inelastic Scattering (TDIS), approved Jefferson Lab experiment C12-15-006A (2015).
- [21] A. C. Aguilar et al., Eur. Phys. J. **A55**, 190 (2019), 1907.08218.
- [22] X. Ji, Phys. Rev. Lett. **110**, 262002 (2013), 1305.1539.
- [23] X. Ji, Sci. China Phys. Mech. Astron. **57**, 1407 (2014), 1404.6680.
- [24] H.-W. Lin, J.-W. Chen, S. D. Cohen, and X. Ji, Phys. Rev. **D91**, 054510 (2015), 1402.1462.
- [25] J.-W. Chen, S. D. Cohen, X. Ji, H.-W. Lin, and J.-H. Zhang, Nucl. Phys. **B911**, 246 (2016), 1603.06664.
- [26] H.-W. Lin, J.-W. Chen, T. Ishikawa, and J.-H. Zhang (LP3), Phys. Rev. **D98**, 054504 (2018), 1708.05301.
- [27] C. Alexandrou, K. Cichy, V. Drach, E. Garcia-Ramos, K. Hadjiyiannakou, K. Jansen, F. Steffens, and C. Wiese, Phys. Rev. **D92**, 014502 (2015), 1504.07455.
- [28] C. Alexandrou, K. Cichy, M. Constantinou, K. Hadjiyiannakou, K. Jansen, F. Steffens, and C. Wiese, Phys. Rev. **D96**, 014513 (2017), 1610.03689.
- [29] C. Alexandrou, K. Cichy, M. Constantinou, K. Hadjiyiannakou, K. Jansen, H. Panagopoulos, and F. Steffens, Nucl. Phys. **B923**, 394 (2017), 1706.00265.
- [30] J.-W. Chen, T. Ishikawa, L. Jin, H.-W. Lin, Y.-B. Yang, J.-H. Zhang, and Y. Zhao, Phys. Rev. **D97**, 014505 (2018), 1706.01295.
- [31] Y.-S. Liu, J.-W. Chen, L. Jin, R. Li, H.-W. Lin, Y.-B. Yang, J.-H. Zhang, and Y. Zhao (2018), 1810.05043.
- [32] H.-W. Lin, J.-W. Chen, X. Ji, L. Jin, R. Li, Y.-S. Liu, Y.-B. Yang, J.-H. Zhang, and Y. Zhao, Phys. Rev. Lett. **121**, 242003 (2018), 1807.07431.
- [33] H.-W. Lin and R. Zhang, Phys. Rev. **D100**, 074502 (2019).
- [34] J.-H. Zhang, J.-W. Chen, L. Jin, H.-W. Lin, A. Schfer, and Y. Zhao, Phys. Rev. **D100**, 034505 (2019), 1804.01483.
- [35] J.-W. Chen, H.-W. Lin, and J.-H. Zhang (2019), 1904.12376.
- [36] J.-H. Zhang, J.-W. Chen, X. Ji, L. Jin, and H.-W. Lin, Phys. Rev. **D95**, 094514 (2017), 1702.00008.
- [37] J.-H. Zhang, L. Jin, H.-W. Lin, A. Schfer, P. Sun, Y.-B. Yang, R. Zhang, Y. Zhao, and J.-W. Chen (LP3), Nucl. Phys. **B939**, 429 (2019), 1712.10025.
- [38] J.-W. Chen, L. Jin, H.-W. Lin, Y.-S. Liu, Y.-B. Yang, J.-H. Zhang, and Y. Zhao (2018), 1803.04393.
- [39] S. Dulat, T.-J. Hou, J. Gao, M. Guzzi, J. Huston, P. Nadolsky, J. Pumplin, C. Schmidt, D. Stump, and C. P. Yuan, Phys. Rev. **D93**, 033006 (2016), 1506.07443.
- [40] R. D. Ball et al. (NNPDF), Eur. Phys. J. **C77**, 663 (2017), 1706.00428.
- [41] A. Accardi, L. T. Brady, W. Melnitchouk, J. F. Owens, and N. Sato, Phys. Rev. **D93**, 114017 (2016), 1602.03154.
- [42] E. R. Nocera, R. D. Ball, S. Forte, G. Ridolfi, and J. Rojo (NNPDF), Nucl. Phys. **B887**, 276 (2014), 1406.5539.
- [43] J. J. Ethier, N. Sato, and W. Melnitchouk, Phys. Rev. Lett. **119**, 132001 (2017), 1705.05889.
- [44] R. Zhang, Z. Fan, R. Li, H.-W. Lin, and B. Yoon, Phys. Rev. **D101**, 034516 (2020), 1909.10990.
- [45] Y.-Q. Ma and J.-W. Qiu, Phys. Rev. **D98**, 074021 (2018), 1404.6860.
- [46] Y.-Q. Ma and J.-W. Qiu, Phys. Rev. Lett. **120**, 022003 (2018), 1709.03018.
- [47] A. V. Radyushkin, Phys. Rev. **D96**, 034025 (2017), 1705.01488.
- [48] K.-F. Liu and S.-J. Dong, Phys. Rev. Lett. **72**, 1790 (1994), hep-ph/9306299.
- [49] J. Liang, K.-F. Liu, and Y.-B. Yang, EPJ Web Conf. **175**, 14014 (2018), 1710.11145.
- [50] W. Detmold and C. J. D. Lin, Phys. Rev. **D73**, 014501 (2006), hep-lat/0507007.
- [51] V. Braun and D. Miller, Eur. Phys. J. **C55**, 349 (2008), 0709.1348.
- [52] G. S. Bali et al., Eur. Phys. J. **C78**, 217 (2018), 1709.04325.
- [53] A. J. Chambers, R. Horsley, Y. Nakamura, H. Perlt, P. E. L. Rakow, G. Schierholz, A. Schiller, K. Somfleth, R. D. Young, and J. M. Zanotti, Phys. Rev. Lett. **118**, 242001 (2017), 1703.01153.
- [54] E. Follana, Q. Mason, C. Davies, K. Hornbostel, G. P. Lepage, J. Shigemitsu, H. Trottier, and K. Wong (HPQCD, UKQCD), Phys. Rev. **D75**, 054502 (2007), hep-lat/0610092.
- [55] A. Bazavov et al. (MILC), Phys. Rev. **D87**, 054505 (2013), 1212.4768.
- [56] I. W. Stewart and Y. Zhao, Phys. Rev. **D97**, 054512 (2018), 1709.04933.
- [57] A. Hasenfratz and F. Knechtli, Phys. Rev. **D64**, 034504 (2001), hep-lat/0103029.
- [58] R. Gupta, Y.-C. Jang, H.-W. Lin, B. Yoon, and T. Bhattacharya, Phys. Rev. **D96**, 114503 (2017), 1705.06834.
- [59] T. Bhattacharya, V. Cirigliano, S. Cohen, R. Gupta, A. Joseph, H.-W. Lin, and B. Yoon (PNDME), Phys. Rev. **D92**, 094511 (2015), 1506.06411.
- [60] T. Bhattacharya, V. Cirigliano, R. Gupta, H.-W. Lin, and B. Yoon, Phys. Rev. Lett. **115**, 212002 (2015), 1506.04196.
- [61] T. Bhattacharya, S. D. Cohen, R. Gupta, A. Joseph, H.-W. Lin, and B. Yoon, Phys. Rev. **D89**, 094502 (2014), 1306.5435.
- [62] R. Babich, J. Brannick, R. C. Brower, M. A. Clark, T. A. Manteuffel, S. F. McCormick, J. C. Osborn, and C. Rebbi, Phys. Rev. Lett. **105**, 201602 (2010), 1005.3043.
- [63] J. C. Osborn, R. Babich, J. Brannick, R. C. Brower, M. A. Clark, S. D. Cohen, and C. Rebbi, PoS **LAT-TICE2010**, 037 (2010), 1011.2775.
- [64] R. G. Edwards and B. Joo (SciDAC, LHPC, UKQCD), Nucl. Phys. Proc. Suppl. **140**, 832 (2005), [832(2004)], hep-lat/0409003.
- [65] G. S. Bali, B. Lang, B. U. Musch, and A. Schfer, Phys.

- Rev. **D93**, 094515 (2016), 1602.05525.
- [66] M. Constantinou and H. Panagopoulos, Phys. Rev. **D96**, 054506 (2017), 1705.11193.
- [67] J.-W. Chen, T. Ishikawa, L. Jin, H.-W. Lin, J.-H. Zhang, and Y. Zhao (LP3), Chin. Phys. **C43**, 103101 (2019), 1710.01089.
- [68] T. Izubuchi, L. Jin, C. Kallidonis, N. Karthik, S. Mukherjee, P. Petreczky, C. Shugert, and S. Syritsyn, Phys. Rev. **D100**, 034516 (2019), 1905.06349.
- [69] M. Oehm, C. Alexandrou, M. Constantinou, K. Jansen, G. Koutsou, B. Kostrzewa, F. Steffens, C. Urbach, and S. Zafeiropoulos, Phys. Rev. **D99**, 014508 (2019), 1810.09743.
- [70] G. P. Salam and J. Rojo, Comput. Phys. Commun. **180**, 120 (2009), 0804.3755.
- [71] C. Chen, L. Chang, C. D. Roberts, S. Wan, and H.-S. Zong, Phys. Rev. **D93**, 074021 (2016), 1602.01502.
- [72] R. S. Sufian, C. Egerer, J. Karpie, R. G. Edwards, B. Jo, Y.-Q. Ma, K. Orginos, J.-W. Qiu, and D. G. Richards (2020), 2001.04960.
- [73] A. Watanabe, T. Sawada, and C. W. Kao, Phys. Rev. **D97**, 074015 (2018), 1710.09529.
- [74] M. Gluck, E. Reya, and M. Stratmann, Eur. Phys. J. **C2**, 159 (1998), hep-ph/9711369.
- [75] T. Nguyen, A. Bashir, C. D. Roberts, and P. C. Tandy, Phys. Rev. **C83**, 062201 (2011), 1102.2448.
- [76] J. Lan, C. Mondal, S. Jia, X. Zhao, and J. P. Vary, Phys. Rev. Lett. **122**, 172001 (2019), 1901.11430.
- [77] J. Lan, C. Mondal, S. Jia, X. Zhao, and J. P. Vary, Phys. Rev. **D101**, 034024 (2020), 1907.01509.
- [78] K. D. Bednar, I. C. Clot, and P. C. Tandy, Phys. Rev. Lett. **124**, 042002 (2020), 1811.12310.